INTERACTIONS BETWEEN METAL SURFACES AND SULFUR-CONTAINING AMINO ACIDS

A Thesis Submitted to
the Graduate School of Engineering and Sciences of
İzmir Institute of Technology
in Partial Fulfillment of the Requirements for the Degree of

MASTER OF SCIENCE

in Physics

by
Mustafa Çevlikli

July 2022
İZMİR

ACKNOWLEGMENTS

I would like to thank my supervisor Asst. Prof. Dr. Evren ATAMAN for all of his contribution, guidance and support.

Also, I would like to thank Asst. Prof. Dr. Emre SARI and Prof. Dr. Lütfi ÖZYÜZER for opening their labs for our study.

I want to thank Res. Asst. Metin TAN for his assistance at laboratory. Also, I want to thank my friend Simon KARABULUT.

This study has been accepted and supported by BAP program as Project: 2021İYTE-1-0099. I want to thank IYTE-BAP committee for their support.

I am thankful to the committee members Asst. Prof. Dr. Günnur GÜLER and Asst. Prof. Dr. Fatma Pınar Gördesli DUATEPE.

ABSTRACT

INTERACTIONS BETWEEN METAL SURFACES AND SULFUR-CONTAINING AMINO ACIDS

With Covid-19 pandemic, the scientific studies over viruses gained a big acceleration. Some of these studies show that SARS-CoV-2 can infect through direct ways from a patient. Besides that, surfaces that are contaminated from adsorption of the virus can indirectly infect a person. Because of this, the studies on the interaction between viruses and environment is an important field on virus studies.

Spike proteins which project out from protective structure called lipid bilayer and they are outmost elements of SARS-CoV-2 viruses. Spike proteins play a vital role on functions like viral entry to the host cell and attachment to the surfaces. Purpose of this study is to contribute to the existing knowledge about surface interaction of these proteins which have an important role on virus-surface interactions. Because of the complicated physical and chemical form of proteins, in this study, the interaction of amino acids, which are building block of proteins, with metal surfaces are investigated.

0.01M, 0.02M and 0.05M L-cysteine and L-methionine aqueous solution was dropped to the metals frequently used in daily life, chrome (Cr) and iron (Fe) polycrystalline substrates and left to dry out at room temperature and under atmospheric conditions. Since the water solubility of L-cystine is low, only a saturated solution of L-cystine was prepared and same process was applied. After, dried out samples were analyzed with x-ray photoelectron spectroscopy (XPS).

Functional sulfur groups on L-cysteine/Cr, L-methionine/Cr and L-Methionine/Fe system stayed intact. On the other hand, sulfur atoms on L-Cysteine/Fe system oxidized and formed $-SO_x$ species. While all other systems behaved oppositely, the amount of protonated functional amino species ($-NH_3^+$) on L-methionine/Fe system decreased relative to functional amino group ($-NH_2$) with increase in coverage. Due to surface amino acid interaction of L-methionine in different substrates, binding energy of sulfur on iron was measured 1 eV lower than on chromium. In L-cystine/Cr system, while disulfide bonds stayed intact, $-NH_2$ and $-NH_3^+$ functional groups were observed on the surface together.

ÖZET

SÜLFÜR İÇEREN AMİNO ASİTLERİN METAL YÜZEYLERLE ETKİLEŞİMLERİ

COVID-19 pandemisiyle birlikte virüsler hakkında yapılan bilimsel araştırmalar büyük bir hız kazandı. SARS-CoV-2 temelde hava yoluyla bulaşan bir virüstür fakat yapılan bazı çalışmalar virüslerin yüzeylere tutunup belirli bir zaman aralığında bu yüzeylere temas eden kişilere de bulaşabilme ihtimalinin olduğunu ortaya koymuştur. Bu nedenle virüslerin yüzeylerle etkileşimlerinin incelenmesi bu araştırmalar içerisinde önemli bir alan olarak karşımıza çıkmaktadır.

Diken proteinler SARS-CoV-2 virüsünün dış çeperinde bulunan koruyucu lipit zarına bağlı ve diken gibi dışarı doğru çıkan yapılardır. Virüslerin konak hücreye girmesi ve farklı yüzeylere tutunması gibi süreçlerde diken proteinler birinci derecede rol üstlenmektedir. Bu çalışmanın amacı, virüs-yüzey etkileşimlerinde kilit rol oynayan bu proteinlerin yüzeylerle etkileşimleri konusunda var olan bilgi birikimine katkı sağlamaktır. Proteinlerin karmaşık fiziksel ve kimyasal yapılarından dolayı, bu çalışmada, proteinlerin yapıtaşları olan amino asitlerin, metal yüzeylerle etkileşimleri incelenmiştir.

Günlük hayatta sıkça kullanılan metallerden krom (Cr) ve demirin (Fe) polikristal alt taşları üzerine 0.01 M, 0.02 M ve 0.05 M derişimlerinde L-sistein ve L-metiyonin sulu çözeltileri damlatılıp, oda sıcaklığında ve atmosferik ortamda kurumaya bırakıldı. Çözünürlüğü daha düşük olan L-sistin bileşiği ile sadece doymuş bir çözelti hazırlanarak aynı işlemler yapıldı. Çözeltiler kuruduktan sonra örnekler aşırı yüksek vakum (UHV) sistemine konuldu ve x-ışını fotoelektron spektroskopisi (XPS) yöntemi ile analiz edildi.

L-sistein/Cr, L-metiyonin/Cr ve L-metiyonin/Fe sistemlerinde moleküllerde bulunan sülfür içeren fonksiyonel gruplar bozulmazken, L-sistein/Fe sisteminde $-SO_x$ türünde sülfür gözlemlendi. Diğer sistemler tam tersi davranış sergilerken, L-metiyonin/Fe sisteminde proton kazanmış amino fonksiyonel grubunun ($-NH_3^+$) miktarının yüzeydeki molekül miktarıyla birlikte amino grubuna ($-NH_2$) göre azaldığı gözlendi. L-metiyonindeki sülfür atomunun yüzey etkileşimleri sebebiyle Fe alt taşta, Cr'ye göre 1 eV daha düşük bağlanma enerjisi ölçüldü. L-sistin/Cr sisteminde disülfür bağları korunurken, yüzeyde $-NH_2$ ve $-NH_3^+$ fonksiyonel grupları birlikte gözlemlendi.

TABLE OF CONTENTS

LIST OF FIGURES

Figure **Page**

LIST OF TABLES

Figure **Page**

CHAPTER 1

INTRODUCTION

After Covid-19 is defined as a pandemic[1], viruses became a hot topic worldwide. The tiny infectious agents, viruses, can only be reproductive if they infect a host cell.[2] Viruses own a nucleic acid protected by a protein-made exterior surface called capsid or nucleocapsid.[3] Some viruses, such as influenza, have an extra protective structure called envelope (a lipid-bilayer) and this kind of viruses is called enveloped viruses. Enveloped viruses can have a structure called spike protein that is projecting out from the envelope of the virion.[4]

The size of viruses can vary from 20 nm to 500 nm in diameter. However, the more common size for a virion is about 50 nm to 100 nm.[5] Viruses can also vary in shape. Helical or rod shape viruses, polyhedral viruses, spherical viruses and complex viruses are the main geometrical formations. Another important property of viruses is the genetic material of the virion. Depending on the genetic material they carry, viruses can be separated into two branches; DNA viruses and RNA viruses.

Viruses are responsible for 60% of all infections of humans.[6] This shows how important it is to understand the spreading mechanism of viruses. Disease transmission can occur in direct or indirect ways.[7] While direct transmission happens via physical contact or droplet spread, indirect transmission is the transfer of microorganism through objects. An example of indirect transmission is contacting a surface which is contaminated by an infected person.

Severe acute respiratory syndrome coronavirus 2 (SARS-CoV-2), is the virus which started the pandemic in 2019.[8] Studies on SARS-CoV-2 show that the virus can live on plastic and stainless steel surfaces for 3 days, on copper for 4 hours, and on cardboard for 1 day.[8] Even though there are objections to the infectibility of viruses from surfaces to humans,[9] it is an important issue to understand virus-surface interactions. While we have a lot of information gap about the infectibility of SARS-CoV-2 virus transmitted through indirect ways[10], pandemic days showed that virus surface interaction can have a significant effect even in our daily routines.

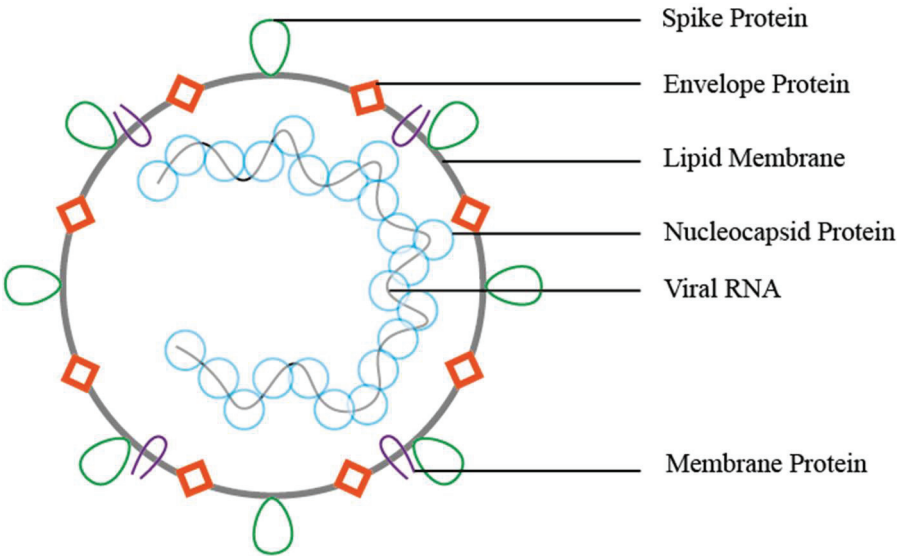

Figure 1.1. Structure of Coronavirus

In Figure 1.1 the structural elements of coronavirus are shown. Coronaviruses are RNA viruses that have a virion about 125 nm in diameter.[11] The SARS-CoV-2 virus is an enveloped virus that has spike proteins which are formed by 1273 amino acids.[12] Membrane of coronavirus has three different proteins which are the envelope protein (E), the membrane protein (M) and the spike protein (S). Spike protein gives SARS-CoV-2 the talent of binding host cells. [13]. Besides binding to cells, as the spike protein is the outmost element of the virus, its structural features provide great importance for understanding virus-surface interactions.[14]

For coronavirus, spike proteins are responsible for the first interaction of virion with the outer world. Attachment to the surfaces and viral entry to the host cell depend on the virion's spike protein structure. Not only for coronavirus but for every enveloped virion that is investigated, the protein is responsible for the first interactions of the virus and outer world like adsorption on the surface or entrance to the cell.[15]

Amino acids are one of the most basic biomolecules and they play a role as the elementary unit to build organic structures like proteins.[16] Even though there are over 140 amino acids in protein structure in nature, most of them are the modification of 20 canonical amino acids.[17] For this reason understanding amino acid-surface interaction can be an important step to understanding virus-surface interactions. As an essential amino acid, L-methionine must be taken through dietary way. However, L-cysteine is produced from L-methionine by a metabolic process.[18] Beside their metabolic importance these two

amino acids also have significant roles in protein structure. L-methionine is the protein construction starter amino acid for eukaryotic cells. Also, as one of the most hydrophobic amino acid, L-methionine is usually found in the core of spherical proteins, and the transmembrane protein in which it interacts with phospholipid bilayer. On the other hand, L-cysteine has significant importance because of its capability of forming disulfide ($-S-S-$) bonds without the help of enzymes. With this property L-cysteine forms inter and intra disulfide bonds in the proteins and plays a vital role in protein folding mechanism.[19]

Even though their importance, spike proteins are very complicated biological structures to study with x-ray photoelectron spectroscopy (XPS). Therefore, in this thesis, we investigated adsorption of sulfur containing amino acids to model protein-surface interactions. The XPS results for the adsorption of three sulfur containing amino acids, L-methionine, L-cysteine and L-cystine, on two metallic surfaces which are widely used in our daily lives, chromium and iron, are shown. Spectral changes depending on coverage are investigated on both substrates and molecules. In total, 12 different solution-substrate combinations have been studied to understand the adsorption process of sulfur-containing amino acids to widely used metallic surfaces.

CHAPTER 2

MATERIALS AND METHODS

2.1 X-ray Photoelectron Spectroscopy (XPS)

In this section history and principle of XPS, experimental setup used in this study and details of experiment is discussed.

2.1.1 A Brief History of XPS

When a material is irradiated with an electromagnetic radiation with proper energy, it emits electrons. These electrons are called photoelectrons and this phenomenon is called photoelectric effect. Photoelectric effect was first observed by Heinrich Rudolf Hertz experimentally in 1887.[20] However, the theoretical explanation stayed as a mystery for almost two decades. German physicist Philipp Eduard Anton von Lenard showed the relationship between the energy of electrons and the frequency of the light. After Philipp Lenard, in 1905, Albert Einstein explained the photoelectric effect and won the Nobel Prize in physics in 1921.

In 1914, Robinson and Rawlinson published the paper “The magnetic spectrum of the β rays excited in metals by soft x-rays”. As seen in the Figure 2.1 soft x-rays are between ultraviolet light and hard x-rays. This was the first-time observation of photoemission by x-ray photons. Steinhardt and Serfass made the first application of this phenomenon.[21] Finally, by the studies of Kai M. Siegbahn, modern spectroscopy technique has been developed. Kai M. Siegbahn was honored with the Nobel Prize in physics in 1981 for his contributions to high-resolution electron spectroscopy.

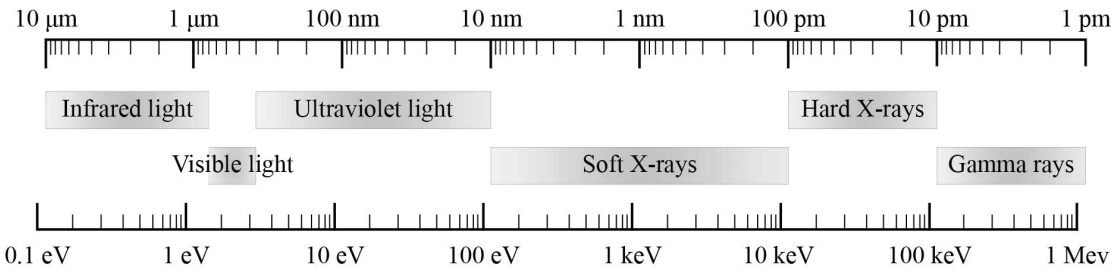

Figure 2.1. Electromagnetic spectrum

2.1.2 Principles of XPS

X-ray photoelectron spectroscopy is a semiquantitative spectroscopic technique that is surface sensitive and based on photoelectric effect. In XPS soft x-rays are used to excite the electrons of the sample. When the excited electrons leave the sample, the analyzer of XPS instrument measures the kinetic energy of emitted electrons[20] and this provides the information of binding energies. The mathematical expression for this process is given in Eq. 2.1

$$E_{binding} = E_{photon} - (E_{kinetic} + \Phi_{spec}) \qquad \text{(Eq. 2. 1)}$$

In the Eq. 2.1, E_{photon} is the energy of x-ray photons, $E_{binding}$ stands for the binding and $E_{kinetic}$ stands for the kinetic energy of the electron and the Φ_{spec} is the work function of the spectrometer. Work function is the minimum amount of energy that is needed to remove an electron from the surface of a solid material in vacuum.[22]

Electrons in an atom are attracted to the nucleus. This attraction creates the binding energy of an electron. To break this bond, electrons need to be stimulated with an energy higher than the binding energy. This stimulation can be created by photons.

The x-ray source in an XPS instrument is the part that generates x-ray photons. The energy of x-ray photons depends on the material of the x-ray source. The most commonly used x-ray sources for laboratory-based XPS devices are aluminum and magnesium.[23] Corresponding photon energy for aluminum source is 1487 eV and for magnesium is 1254 eV. Some other x-ray sources are titanium and chromium with a photon energy of 4510 eV and 5417 eV, respectively. As an example, when an x-ray photon with 1487 eV energy hits an electron with 250 eV binding energy, it roughly gains a kinetic energy of 1237 eV.

Although the soft x-rays can penetrate, in average, a few micrometers deep, XPS technique can only collect data from roughly the first 10 nm of the sample.[20] That is why it is called a surface sensitive technique. There are four commonly used concepts to express the surface sensitivity.[24] The inelastic mean free path (IMFP) is defined as the distance an electron can travel without an elastic collision. As an example, the inelastic mean free path for an electron with 1500 eV kinetic energy is around 20 angstrom in Cu.[25] The effective attenuation length (EAL) differs from the inelastic mean free path by taking account of inelastic collisions as well. The mean escape depth (MED) is the mean deepness that a photoelectron can escape from the surface, and the information depth (ID) is the deepest point we can get meaningful information.

When an electron is excited, it has a certain probability to leave the material surface without losing any kinetic energy. Once the electrons leave the surface of the sample, their kinetic energy is measured by a hemispherical electron energy analyzer. Hemispherical electron energy analyzer is a device that has two concentric hemispheres with a voltage difference. This way it bends the trajectory of the electron depending on its kinetic energy. Once kinetic energy of the electron is measured, difference between photon energy and kinetic energy gives us the binding energy.

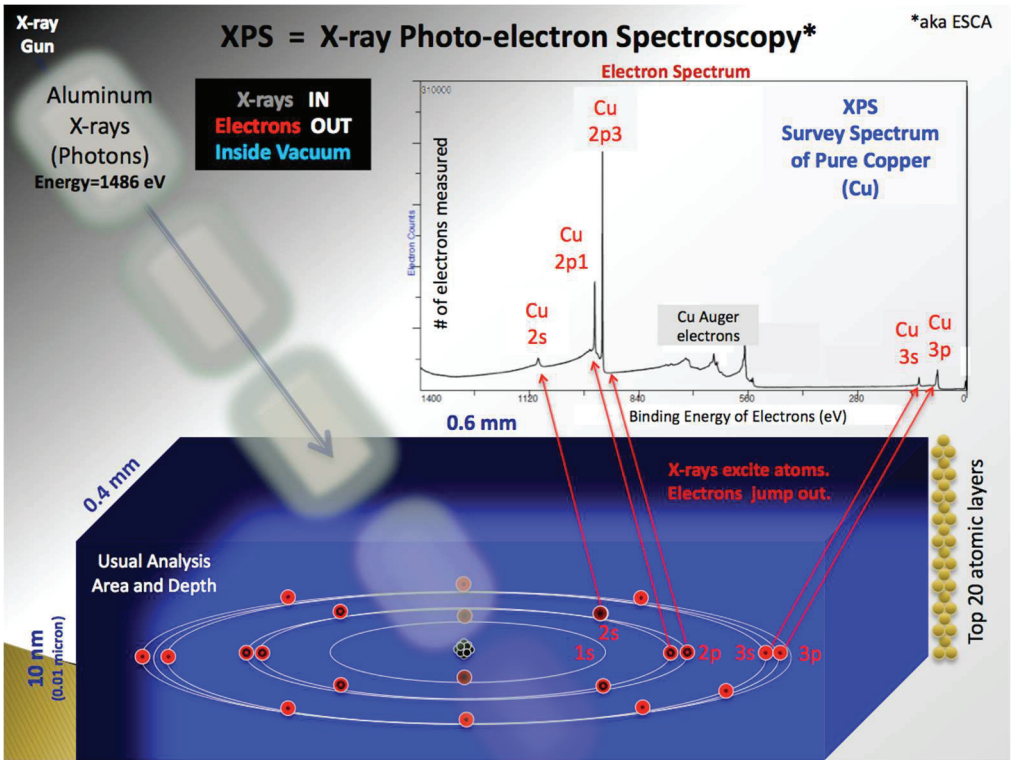

Figure 2.2. Basic Principle of XPS[26]

In the Figure 2.2 basic physical principle of XPS is shown. X-ray photons are absorbed by electrons, and they gain a kinetic energy. By measuring their kinetic energy, we can infer the binding energy of the electron. Different orbitals have different binding energies and XPS has the ability to detect which electrons are coming from what orbital.

2.1.3 Determination of Elemental Composition

XPS can determine what elements comprise a sample's surface except hydrogen and helium. Atom's core structure and its electron organization change the spectral properties of the elements. Therefore, every element has its own characteristic footprint on XPS spectra. This mechanism provides enough information to understand which elements are present in the sample's surface. Figure 2.3 shows an example of XPS spectrum that we have measured for L-cystine molecules adsorbed on Cr substrate.

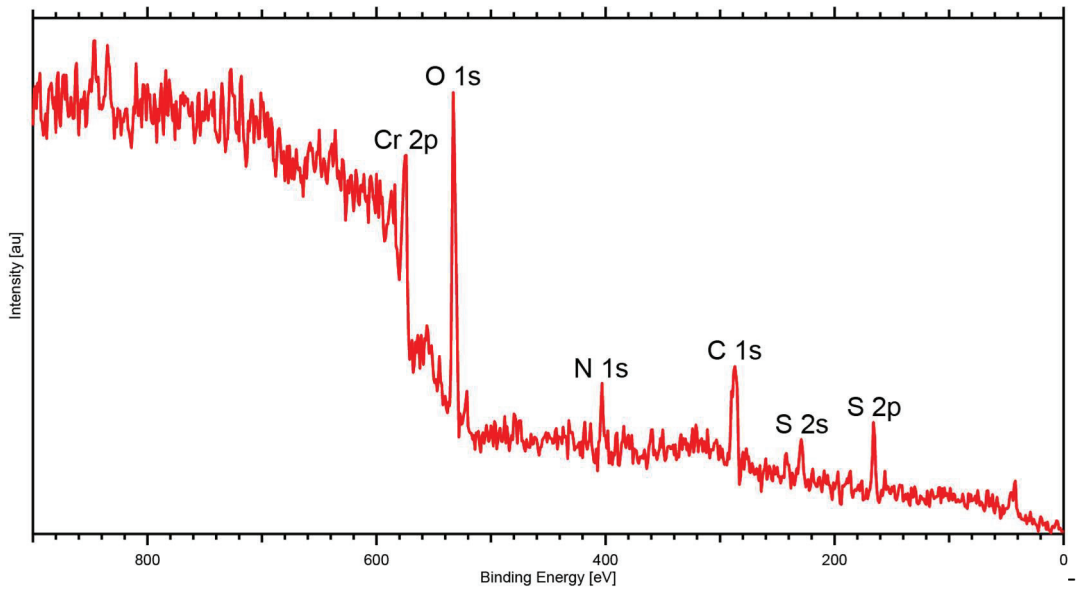

Figure 2.3. Survey spectra of L-cystine on chromium sample

2.1.4 Determination of Chemical Environment

The data that XPS provides not only gives information about the elemental composition but also gives information about the chemical environment that the elements

exist in. In the following tables there are some examples from literature for binding energy interval of carbon and oxygen in different chemical environments.[27]

Table 2.1. Some examples of C1s binding energies with different surrounding atoms.

Chemical State	**C 1s Binding Energy (eV)**
C	284.2 – 285.0
$C-N$	285.5 – 288.4
$C=O$	288.0 – 289.2
$C-S$	285.4 – 287.4

Table 2.2. Some examples of O1s binding energy with different surrounding atoms.

Chemical State	**O 1s Binding Energy (eV)**
$Metal\ Oxides$	528.1 – 531.0
Fe_2O_3	529.6 – 530.2
$Hydroxides$	532.6 – 533.4
$Nitrates$	532.8 – 533.8

As seen in the Table 2.1 and Table 2.2 neighboring atoms have an impact on binding energy. The reason of that is they create an electric potential around the electron one can observe in XPS. Changes in potential affect the kinetic energy of the electrons measured, and they are observed as different peaks ın a spectrum. Another important phenomenon that has an impact on binding energy is oxidation states. The following table shows the binding energy of iron which is changing with the oxidation state shown as an example.[28]

Table 2.3. Some examples of binding energy of Fe with different oxidation states.

Chemical State	**Binding Energy (eV)**
Fe	706.7
FeO	709.6
Fe_3O_4	710.7

2.1.5 Quantification

It is not possible to obtain absolute amounts, but XPS technique can give information of relative amounts of atoms in a samples surface. Besides determination of the atomic concentration, XPS data also gives information about relative concentration of different chemical environment of the atom. In the Table 2.4 the atomic concentration of glutamic acid ($C_5H_9NO_4$) is given.[16]

Table 2.4. Atomic Concentration of Glutamic Acid

Energy Levels	Atomic Concentration	Chemical Bonds
C 1s (1)	20.1%	$C-(C,H)$
C 1s (2)	12.4%	$C-N$
C 1s (3)	20.1%	$O=C-OH$
O 1s (1)	27.2%	$O^{**}=C-OH$
O 1s (2)	10.4%	$O=C-O^{**}H$
N 1s (1)	9.8%	NH_3^+

One of the most challenging part for an XPS data analysis is the curve fitting. The aim of curve fitting is not to find out the best representation of spectra but to find out physical and chemical states of the material.[29] This process requires experience in both XPS and the material under consideration. Same XPS spectra can be represented by different number of components and all of them can be mathematically meaningful while physically different. One of good indicators to test a fitted curve is full width at half maximum (FWHM). FWHM is the wideness of the curve at half of the maximum intensity. While the broad peaks have higher FWHM values they can have numerous contributors, the narrow peaks have lower FWHM values and indicate a more homogeneous sample. Also, any change in sample can cause an increase in the FWHM value. For example, beam damage can move the peaks and that causes the peak to widen.

XPS requires vacuum condition and there are two reasons for that.[30] First one is the increasing the mean free path of the photoelectrons. In vacuum environment the risk of collision between photoelectrons and residual gas atoms is decreased that may cause possible signal losses. The second and more important reason of vacuum requirement is

the surface sensitivity of the technique. In XPS the photoelectrons measured come from the top first couple of atomic layers. That is why, surface contamination changes XPS data drastically. High vacuum condition helps preventing surface contamination.

2.2 Experimental Details

XPS measurements were performed using a commercial instrument from SPECS GmbH. A schematic drawing of the equipment is given in the Figure 2.4.

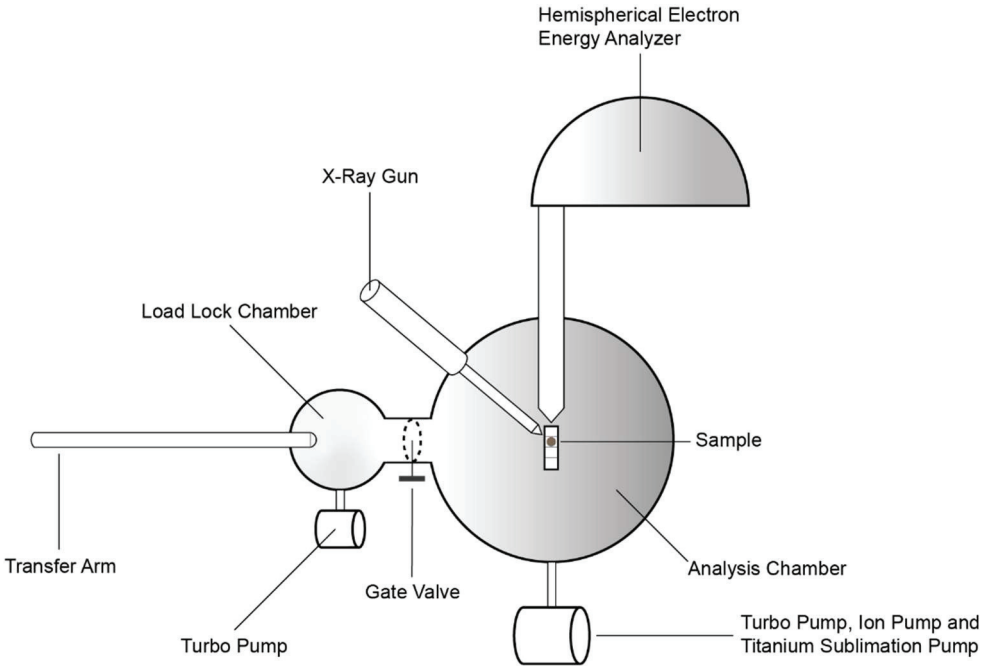

Figure 2.4. Schematic drawing of XPS instrument

The instrument is equipped with a XR50 aluminum/magnesium dual anode x-ray source. Aluminum anode with 1486.6 eV photon energy was used for our measurements. X-ray photons were not monochromatized. The instrument has a hemispherical electron analyzer, PHOIBOS 150 and a 2D CCD detector. A photo of the instrument used in the experiment is shown in Figure 2.5.

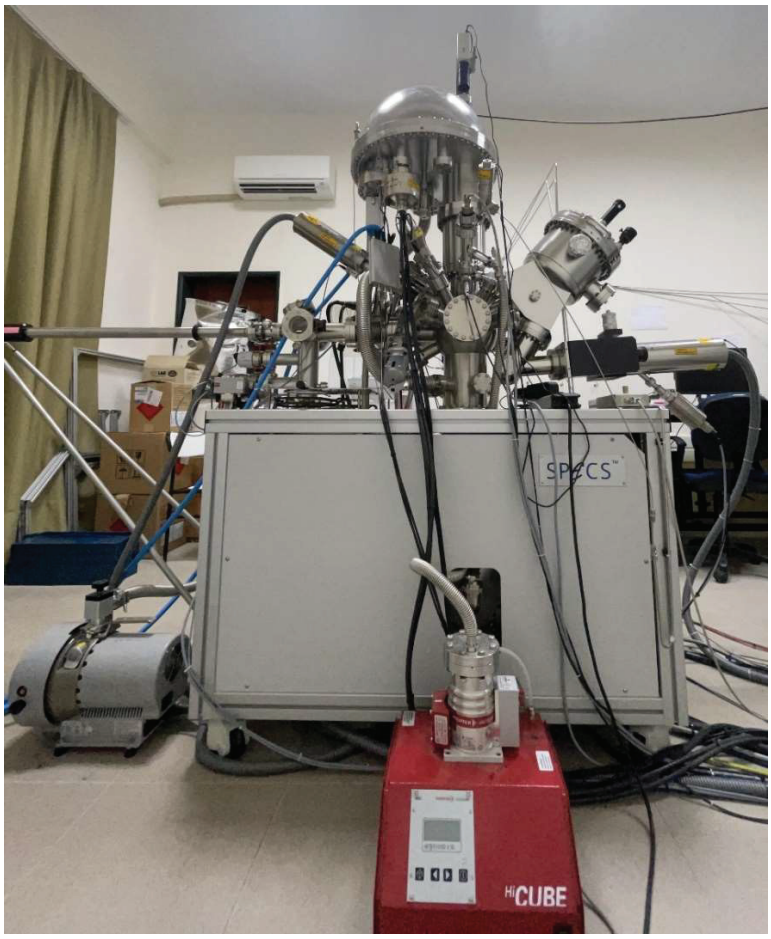

Figure 2.5. XPS equipment used in experiment

Our XPS instrument has two chambers which are an analysis chamber and a load lock. These two chambers are separated by a gate valve. The load lock is pumped by a scroll and a turbo molecular pump. Base pressure at load lock was $3 \times 10^{-8}\ mbar$. In the analysis chamber, there are four pumps: a scroll pump, a turbo molecular pump, an ion pump and a titanium sublimation pump. The base pressure of the analysis chamber was $2 \times 10^{-10}\ mbar$.

Samples are taped to a molybdenum sample holder with double sides carbon adhesive tape and placed to the load lock. Then, they are transferred to the sample manipulator in analysis chamber for analysis.

Sulfur containing amino acids; L-methionine ($C_5H_{11}NO_2S$) with a minimum 98% purity, L-cysteine ($C_3H_7NO_2S$) with a minimum 97% purity and L-cystine ($C_6H_{12}N_2O_4S_2$) with a minimum 98% purity were purchased from Merck Inc. Molecular structure of amino acids are given in Figure 2.6.

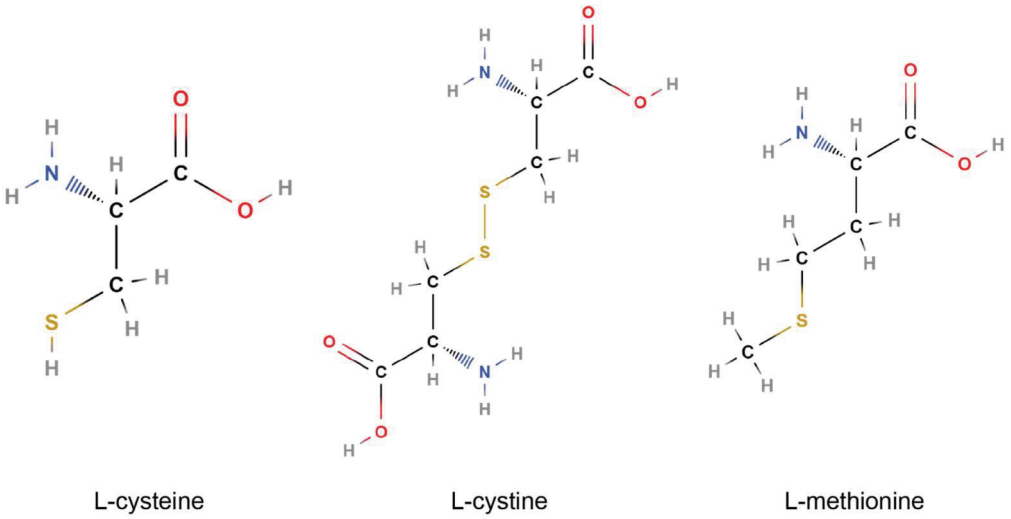

Figure 2.6. 2D Structure of L-cysteine, L-cystine and L-methionine

The polycrystalline chrome and iron substrates were bought from Kurt J. Lesker Co., Ltd. The iron substrate has 99.9% purity, and the chrome substrate has 99.95% purity. Disk shaped substrates were 2.54 cm in diameter and 5 mm thick.

The first measurements of the substrates were conducted as received without any cleaning process. The survey spectra of substrates are displayed as black curves in Figure 2.7 and 2.8. Some adventitious carbon and oxide layers were observed on both metal substrates but we did not observe any other contamination in our samples. Because our plan was to conduct all of our molecule deposition procedures *ex situ,* we did not try to remove this adventitious carbon or oxide layer. However, we have tried to see the effect of our cleaning recipe (explained below) on the substrates. For this purpose, we have applied our cleaning recipe on pristine substrates and we did not observe any significant effect on the amount of carbon and oxygen contamination as seen in the Figure 2.7 and 2.8 as red curves.

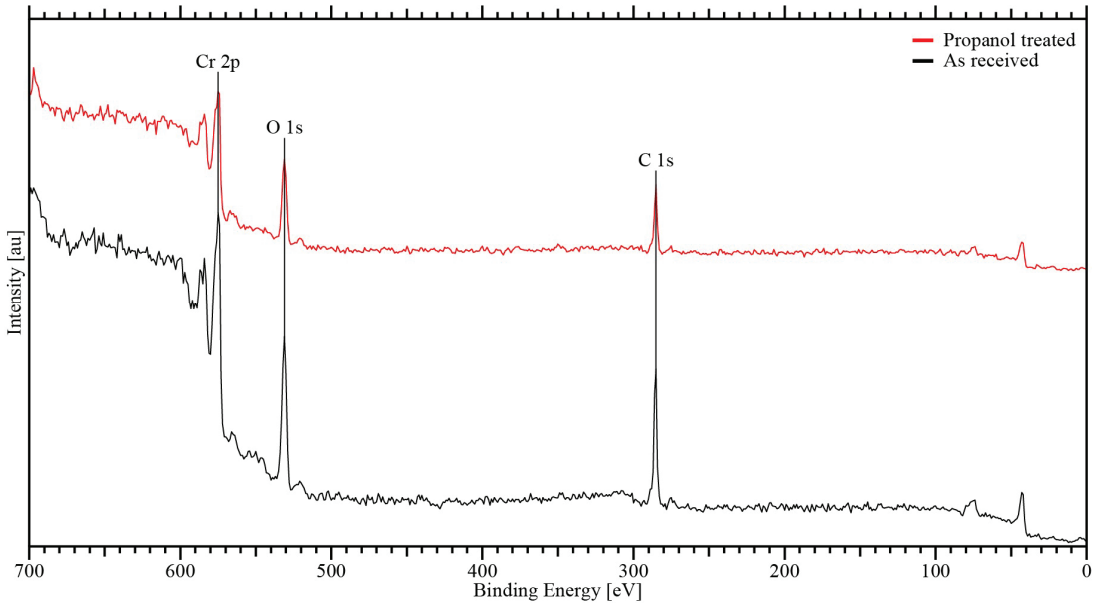

Figure 2.7. As received and propanol treated survey spectra of chromium substrates

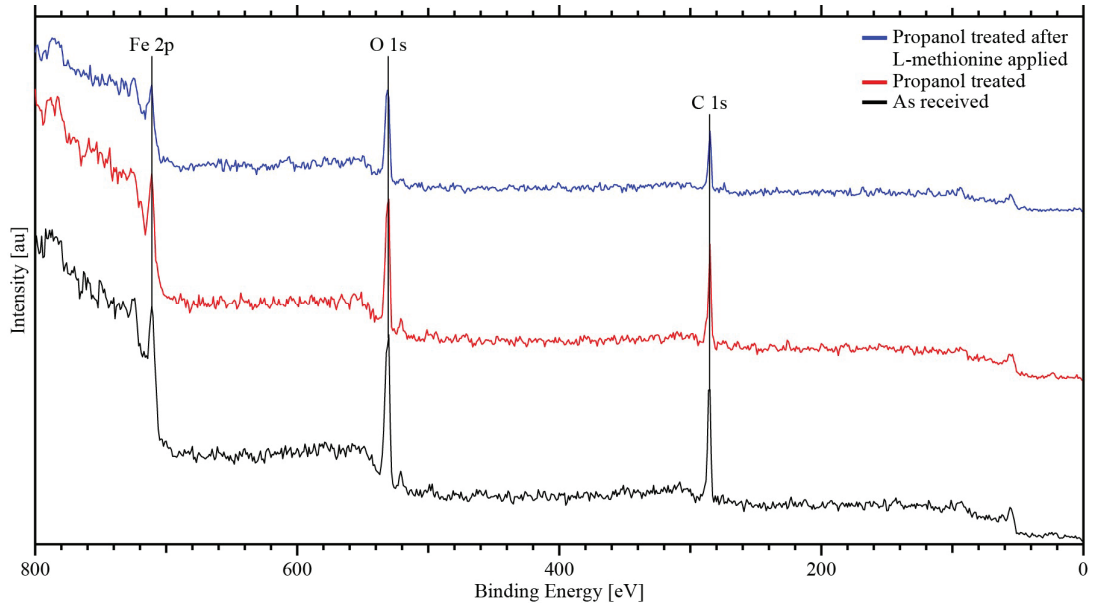

Figure 2.8. As received, propanol treated and after cleaning spectra of iron substrates

Three different concentrations of each amino acid were prepared with distilled water. The solutions of L-methionine, L-cysteine and L-cystine with the concentration of 0.01 M, 0.02 M, 0.05 M were prepared by using a scale with 0.1 mg precision. However, since the water solubility of L-cystine is too low, suspension and precipitation in the solution were observed in a short time after the solution was prepared. For this reason, a specific concentration of L-cystine solution was not used in this study. Instead, a saturated

concentration of L-cystine solution was used. All solutions were stored at 20 ºC temperature and under atmospheric pressure in a tightly sealed amber glass bottle.

Five-six drops of solutions were dropped with a Pasteur pipette onto substrates. A protective plastic cover with ventilation holes was put over to the sample and the sample was left to dry out at 20 °C in atmospheric conditions. Since drops were drying slowly, we expected that concentration of solutions to change during the process. However, in the end, there were three different residuals with different concentrations to compare with each other.

Between measurements for different concentrations, the substrates were rinsed with distilled water and propanol. Followed by a 10 minutes of ultrasonication in distilled water and finally rinsed with water and propanol one more time. Then substrates left drying for couple of hours inside a plastic cover with ventilation holes. We have checked the efficiency of our cleaning recipe with XPS. We measured a sample after cleaning process and we observed no N 1s or S 2p signal and adventitious carbon and oxygen levels were similar. An example of cleaned sample is shown as blue curve in the Figure 2.8.

When 0.05 M L-cysteine and saturated L-cystine solutions were dropped to Fe substrate, a red-purple layer was formed on the surface after the drying process. For this reason, the 0.05 M L-cysteine/Fe and L-cysteine/Fe combinations were excluded. In total, 12 different solution-substrate combinations were studied.

It was observed that some beam damage affected the samples for the first couple of minutes. To eliminate this effect, the first couple of sweeps were not taken into account during the analysis.

CHAPTER 3

RESULTS AND DISCUSSION

3.1 Results

In Figures 3.1–3.4, N 1s and S 2p XP spectra for the three amino acids on the two substrates are shown for different concentrations of droplets. Every spectrum has its tag on top left corner. Black color corresponds to 0.01 M concentration, red color to 0.02 M concentration and blue color to 0.05 M concentration measurements except for the L-cystine/Cr system where the blue color stands for the saturated solution.

A Shirley-type background is used for fitting S 2p spectra. However, for some of the N 1s spectra intensity at the high binding energy side was lower than the intensity at the low binding energy side, therefore, we used a linear background for fitting N 1s spectra. All of our XPS measurements were calibrated to adventitious carbon ($C_x H_y$) peak at 285.0 eV. A Voight line shape is used for fitting different components. Pass energy of the analyzer is set to 50 eV for S 2p and N 1s measurements and to 30 eV for all other measurements.

We adopted the following procedure for fitting the spectra. For a particular molecule-substrate system we used the spectrum with the highest signal-to-noise ratio as a reference. After fitting this spectrum without any constrains we used the resulting FWMH value for all other components for the same molecule-substrate system. For the S 2p spectra we fixed the binding energy of the $2p_{1/2}$ level, 1.2 eV higher than the binding energy of the $2p_{3/2}$ and intensity of the $2p_{1/2}$ level to half of the intensity of $2p_{3/2}$. In this thesis we always refer to $2p_{3/2}$ level when we discuss S 2p spectra.

3.1.1 L-cysteine on Chromium

N 1s and S 2p XP spectra for L-cysteine/Cr system are shown in Figure 3.1. The binding energy, FWHM and relative intensity values for different components are given in Table 3.1.

In N 1s spectra two components were observed for all concentrations. The low binding energy component was named as N1 and high binding energy component was named as N2. Even though the binding energy of both components did not change for the 0.01 M and 0.02 M preparations, both peaks moved to ~0.5 eV higher binding energy for 0.05 M concentration. The relative intensity of the N2 component started with 70.8% for 0.01 M solution and increased with concentration. For the 0.05 M solution, it reached the value of 88.7%.

Only one S 2p doublet was observed in the system (named as S1) for all concentrations. Similar to N 1s, the positions of the doublet did not show a notable change for 0.01 M and 0.02 M concentrations. However, for 0.05 M solution, the peak moved ~0.5 eV toward higher binding energy.

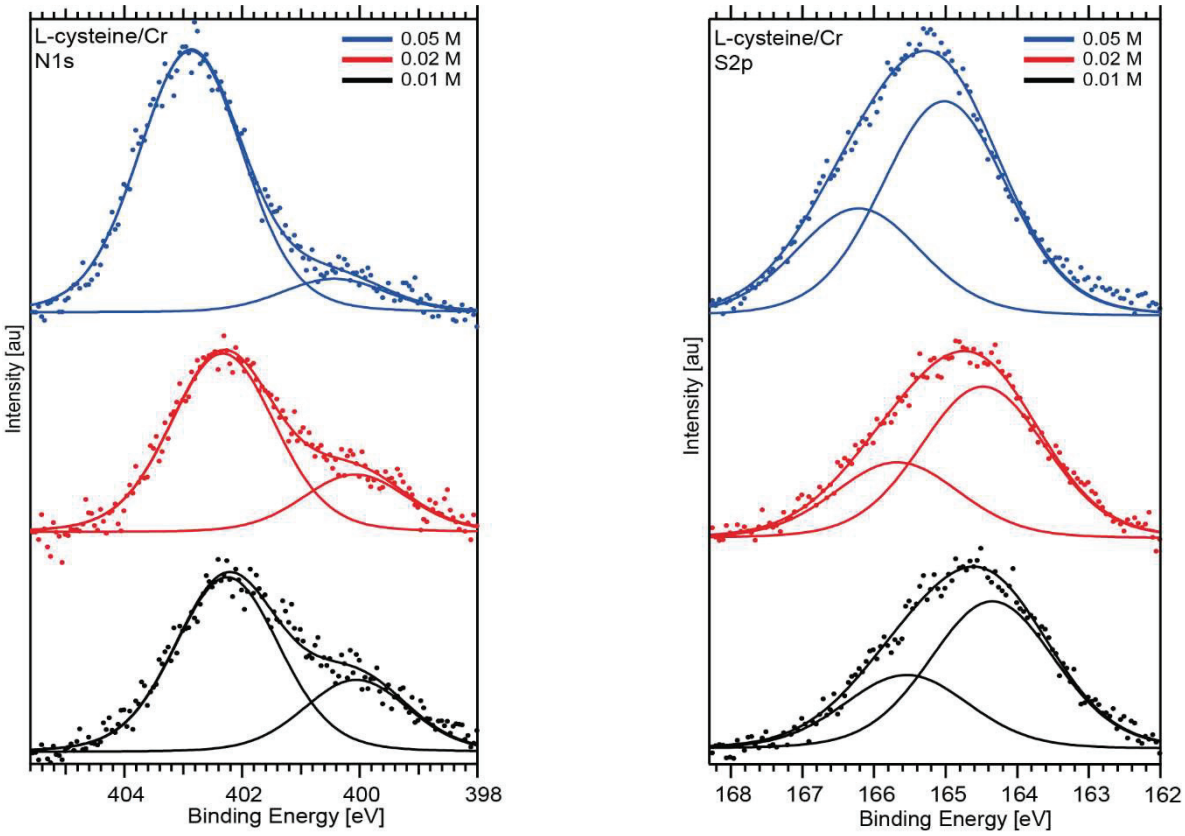

Figure 3.1. High resolution N 1s and S 2p XP spectra of L-cysteine/Cr. Dots represent the measured data and lines show the results of the fitting and individual components.

Table 3.1. Spectral features of L-cysteine on chromium surface

L-cysteine/Cr	N1s	Binding energy (eV)	FWHM (eV)	Area (%)	S $2p_{3/2}$	Binding energy (eV))	FWHM (eV)	Area (%)
0.01M	N1	400.1	2.1	29.2	S1	164.4	2.1	66.7
	N2	402.3	2.1	70.8				
0.02M	N1	400.1	2.1	24.4	S1	164.6	2.1	66.7
	N2	402.4	2.1	75.6				
0.05M	N1	400.5	2.1	11.3	S1	165.1	2.1	66.7
	N2	402.9	2.1	88.7				

3.1.2 L-cysteine on Iron

L-cysteine/Fe experiments were only performed for 0.01 M and 0.02 M concentration values. When 0.05 M solution was dropped on to the iron substrate, it formed a thick red-purple layer. We performed an XPS measurement for this system and results showed a thick layer consisting of Fe, S and O. Therefore, we excluded this concentration from our experiments. The N 1s and S 2p spectra of L-cysteine/Fe system are given in Figure 3.2. The binding energy, FWHM and relative intensity values for different components are given in Table 3.2.

The N 1s components have similar binding energy values compared with L-cysteine/Cr system. However, on iron, N1 component is higher in intensity and decreases with increasing coverage. N1 peak positions did not show a significant difference with concentration for N 1s region. However, N2 peak shifted to higher binding energy by ~0.4 eV.

On the other hand, sulfur had a unique change compared to other systems investigated in this study. For 0.01 M solution we observed only one doublet (S1). But when concentration was increased 0.02 M, a second component (S2) with a binding energy of 166.0 eV emerged. S2 component holds the 14.8% concentration of all sulfurs in the system.

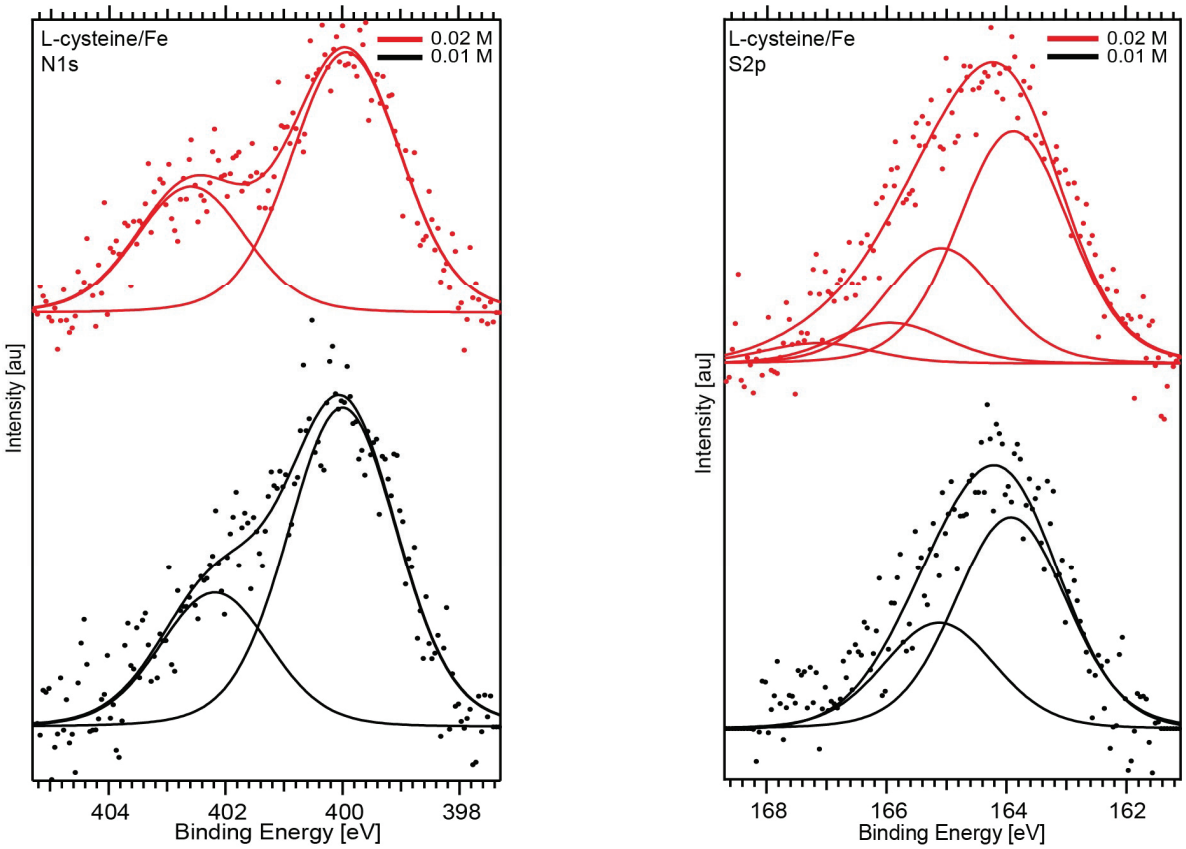

Figure 3.2. High resolution N 1s and S 2p XP spectra of L-cysteine/Fe. Dots represent the measured data and lines show the results of the fitting and individual components.

Table 3.2. Spectral features of L-cysteine on iron surface

L-cysteine/Fe	N 1s	Binding energy (eV))	FWHM (eV)	Area (%)	S $2p_{3/2}$	Binding energy (eV)	FWHM (eV)	Area (%)
0.01M	N1	400.0	2.2	70.4	S1	163.9	2.2	66.7
	N2	402.2	2.2	29.6				
0.02M	N1	400.0	2.2	67.2	S1	163.9	2.2	56.8
	N2	402.6	2.2	32.8	S2	166.0	2.2	9.9

3.1.3 L-methionine on Chromium

L-methionine/Cr XP spectra for N 1s and S 2p are given in Figure 3.3. The binding energy, FWHM and relative intensity values for different components are given in Table 3.3.

N1 and N2 components in N 1s spectrum of L-methionine/Cr system did not show a considerable change in binding energy. On the other hand, ratio of the peaks changed with concentration. With denser solution N2 peak gets more dominant. Same thing is true for the S 2p region. The binding energy of the S1 component do not show a considerable change with increasing coverage.

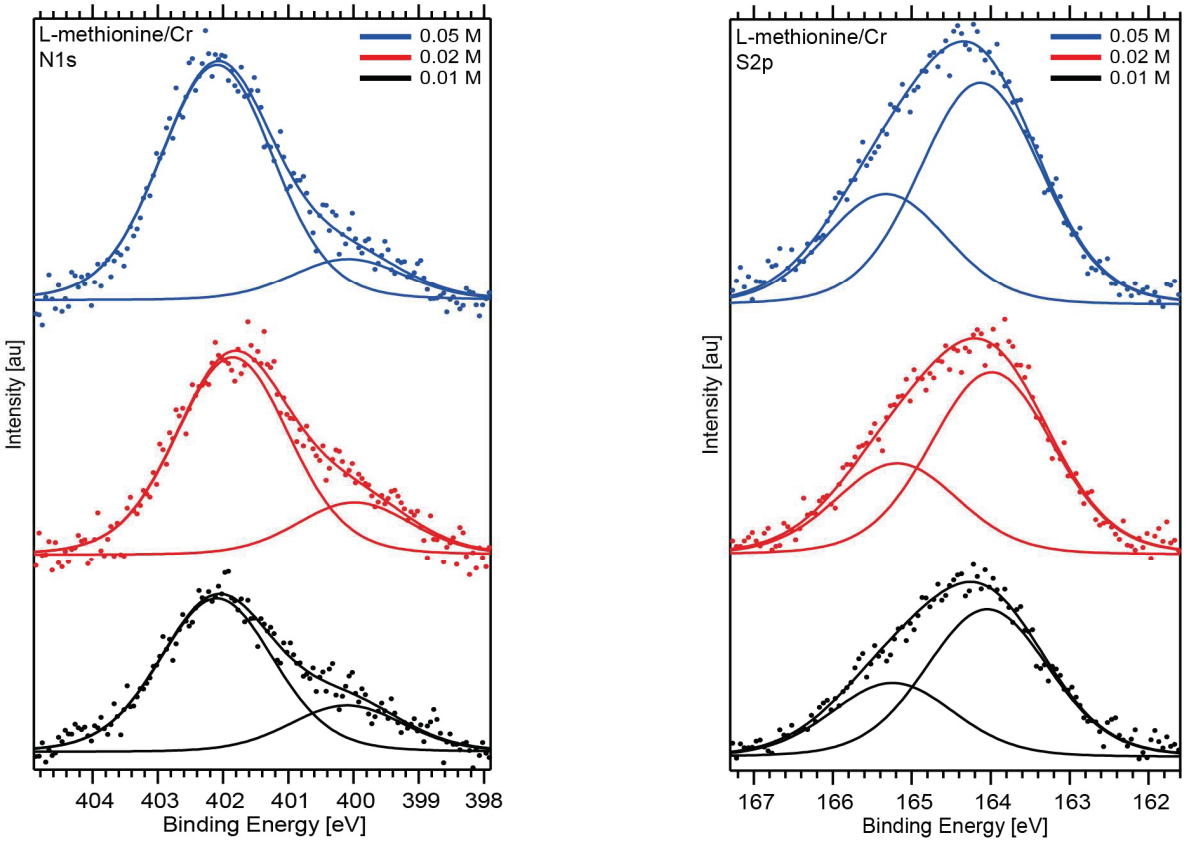

Figure 3.3. High resolution N 1s and S 2p XP spectra of L-methionine/Cr. Dots represent the measured data and lines show the results of the fitting and individual components.

Table 3.3. Spectral features of L-methionine on chromium surface

L-methionine/Cr	N 1s	Binding energy (eV)	FWHM (eV)	Area (%)	S $2p_{3/2}$	Binding energy (eV)	FWHM (eV)	Area (%)
0.01M	N1	400.1	2.0	23.2	S1	164.0	1.8	66.7
	N2	402.1	2.0	76.8				
0.02M	N1	400.0	2.0	21.0	S1	164.0	1.8	66.7
	N2	401.8	2.0	79.0				
0.05M	N1	400.0	2.0	15.0	S1	164.1	1.8	66.7
	N2	402.0	2.0	85.0				

3.1.4 L-Methionine on Iron

N 1s and S 2p spectra of L-methionine/Fe system are shown in Figure 3.4. The binding energy, FWHM and relative intensity values for different components are reported in Table 3.4.

One unique behavior of thıs system is that, at 0.01 M solution, only one N 1s peak (N2) was observed. When the concentration was increased to 0.02 M, a peak with lower binding energy of 399.6 eV appeared (N1). Another unique behavior of L-methionine/Fe system is that N1 getting higher in intensity relative to N2 component with increasing concentration. In the S 2p region only one component (S1) was observed and binding energy did not change with increasing coverage.

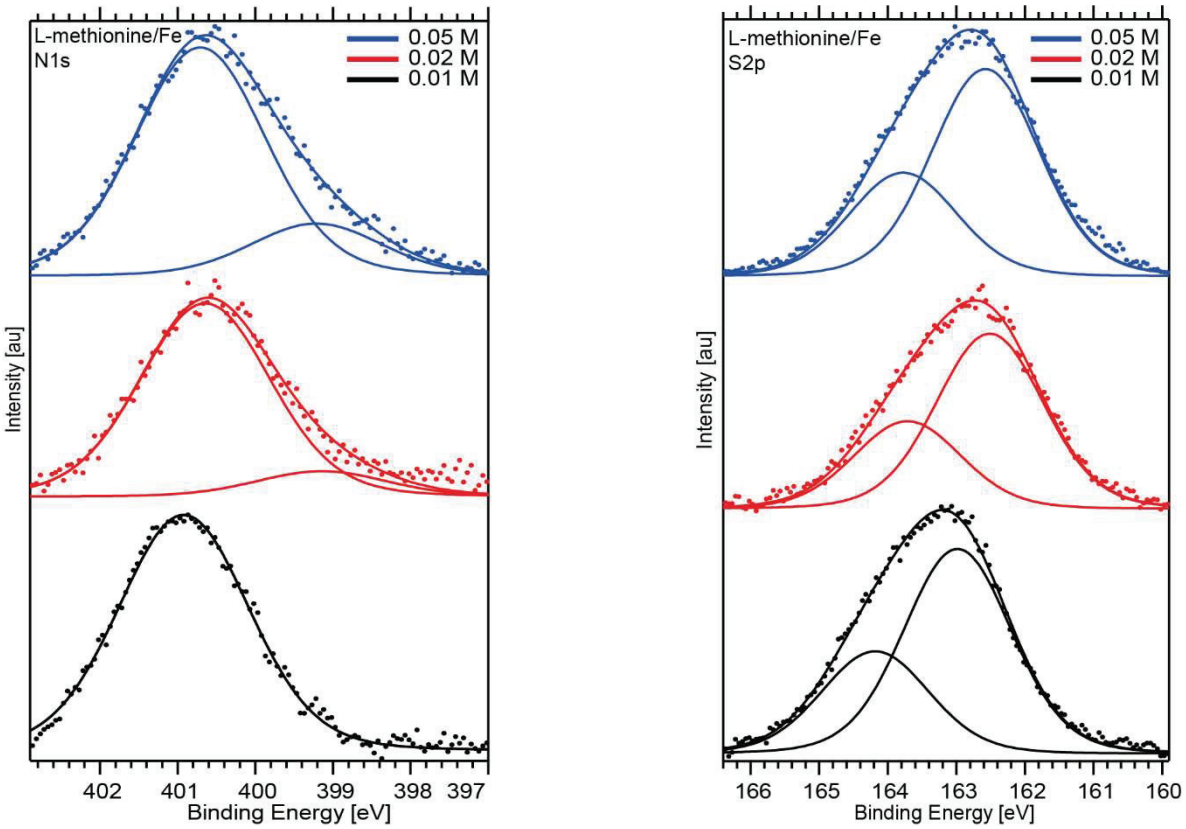

Figure 3.4. High resolution N 1s and S 2p XP spectra of L-methionine/Fe. Dots represent the measured data and lines show the results of the fitting and individual components.

Table 3.4. Spectral features of L-methionine on iron surface

L-methionine/Fe	N 1s	Binding energy (eV)	FWHM (eV)	Area (%)	S $2p_{3/2}$	Binding energy (eV)	FWHM (eV)	Area (%)
0.01M					S1	163.0	1.9	66.7
	N2	400.9	2.0	100.0				
0.02M	N1	399.6	2.0	11.6	S1	163.0	1.9	66.7
	N2	401.1	2.0	88.4				
0.05M	N1	399.5	2.0	18.6	S1	162.9	1.9	66.7
	N2	401.0	2.0	81.4				

3.1.5 L-Cystine on Chromium

L-cystine molecule is only studied for a saturated concentration on chromium substrate. N 1s and S 2p spectra of the system are given in Figure 3.5. The binding energy, FWHM and relative intensity values for different components are given in Table 3.5.

In N 1s region, the higher binding energy component, N2, dominates the spectra with 77.2% relative intensity and S1 component in S 2p region has relatively higher binding energy compared with the other systems that we investigated.

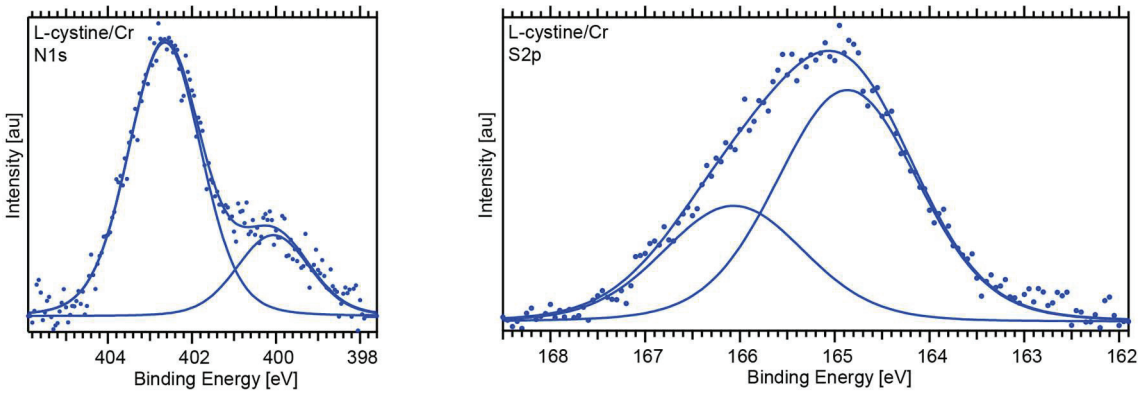

Figure 3.5. High resolution N 1s and S 2p XP spectra of L-cystine/Cr. Dots represent the measured data and lines show the results of the fitting and individual components.

Table 3.5. Spectral features of L-cystine on iron surface

L-cystine/Cr	N 1s	Binding energy (eV)	FWHM (eV)	Area (%)	S $2p_{3/2}$	Binding energy (eV)	FWHM (eV)	Area (%)
Saturated	N1	400.1	2.0	22.8	S1	164.9	1.8	66.7
	N2	402.7	2.0	77.2				

3.2 Literature Review

Because of the importance of amino acids in different areas like medicine, food and drug industry, biochemistry and biotechnology, they are investigated by a lot of researchers from different fields. Even though there is an information gap on iron surfaces-amino acid and chromium surfaces-amino acid interactions, amino acid-metal surface interactions have been studied widely. Studies are mostly centered around of copper and gold substrates and L-cysteine and L-methionine amino acids. A review of literature is given in Table 3.6.

Table 3.6. Literature review **(cont. on next page)**

Ref.	Substrate	Molecule	Binding energy (eV) for different species		Method of Deposition	Adsorption Geometry
31	Polycrystalline Au	L-cysteine	$-S-Au$ $-SH$ $-NH_2$ $-NH_3{}^+$	162.0 eV 163.8 eV 399.3 eV 401.3 eV	UHV & from solution	Dissociative chemisorption through $-SH$ (thiolate). In UHV deposition all amino groups are protonated as $-NH_3{}^+$. In case of adsorption from solution both $-NH_2$ and $-NH_3{}^+$ groups are observed.
32	Polycrystalline Au	L-cysteine	$-S-Au$ $-NH_2$ $-NH_3{}^+$	162.1 eV 399.3 eV 401.3 eV	from solution	SAMs of L-cysteine is formed on Au substrate. Dissociative chemisorption through $-SH$ (thiolate).
33	Polycrystalline Au	L-cysteine	$-S-Au$ $-SH$ $-NH_2$ $-NH_3{}^+$	162.0 eV 164.2 eV 399.5 eV 401.5 eV	UHV & from solution	SAMs of L-cysteine is formed on Au substrate (from solution). A monolayer is composed of a mixture of zwitterions and neutral molecules. For thick multilayers only $-SH$ and $-NH_3{}^+$ species are observed (UHV).
34, 35, 36	Au(111)	L-cysteine	$-S-Au$ $-SH$ $-NH_2$ $-NH_3{}^+$	162.2 eV 164.1 eV 399.6 eV 401.7 eV	from solution	Chemical bond between gold and dissociated $-SH$ (thiolate). There also exist weakly bonded molecules.
37	Au(110)	L-cysteine	$-S-Au$ $-SH$ $-NH_2$ $-NH_3{}^+$	162.0 eV 164.3 eV 399.5 eV 401.5 eV	UHV	Adsorption geometry is very similar to the adsorption geometry on the Au(111) surface. $-NH_3{}^+$ species dominates the monolayer.
38	Au clusters on HOPG	L-cysteine	$-S-Au$ $-SH$ $-NH_2$ $-NH_3{}^+$	162.3 eV 163.8 eV 399.6 eV 401.2 eV	from solution	Chemical bond between gold and $-SH$ (thiolate). $-NH_2$ may also be interacting with gold clusters.
31	Polycrystalline Cu	L-cysteine	$-S-Cu$ $-NH_2$ $-NH_3{}^+$	162.5 eV 399.5 eV 401.2 eV	UHV & from solution	Dissociative chemisorption through the $-SH$ and both $-NH_2$ and $-COOH$ groups are coordinated to the surface. Thiol species is not observed on the surface (from solution).

Table 3.6. Literature review **(cont.)**

33	Polycrystalline Cu	L-cysteine	$-S-Cu$ 162.0 eV $-SH$ 164.2 eV $-NH_2$ 399.5 eV $-NH_3{}^+$ 401.5 eV	UHV	For a monolayer $COO-Cu$, NH_2-Cu bonds are formed in addition to $S-Cu$.
39	Cu(110)	L-cysteine	S_{atomic} 161.3-161.5 eV $-S-Cu$ 162.3 eV $-SH$ 164.3 eV $-NH_2$ 399.6 eV $-NH_3{}^+$ 401.7 eV	UHV	At low coverages $C-S$ bond breaks atomic sulfur is formed. As coverage increases $S-H$ and $O-H$ bonds break and molecules adsorb as thiolates & carboxylates. Later on protonated amino groups form on the surface. Finally, second layer is formed by carboxylate or intact molecules.
40	Cu(110)	L-cysteine L-methionine L-cystine	$-S-Cu$ (1) 161.5 eV $-S-Cu$ (2) 162.3 eV $-SH$ 164.2 eV $-NH_2$ 399.6 eV $-NH_3{}^+$ 401.7 eV	UHV	The thiol group in L-cysteine has the lowest energy gain by the bonding to a Cu atom which results in a relatively high population of the high binding energy thiolate species with increasing coverage. The population of low binding energy thiolate is relatively large throughout the coverage range in L-methionine and L-cystine adsorption. Formation of the zwitterionic state is possible only in adsorbed L-cysteine molecules because of the molecular ordering at the surface.
41	Cu(531)	L-cysteine L-methionine	S_{atomic} ~160.6 eV $-S-Cu$ ~161.7 eV $-SCH_3$ 163.1 eV $-SH$ 163.4 eV $-NH_2$ 399.9 eV $-NH_3{}^+$ 401.7 eV	UHV	At 300 K all functional groups of L-cysteine molecule are attached to the surface but for L-methionine only oxygen atoms and a nitrogen atom interact with the surface.
42	Pt(111)	L-cysteine	$-S-Pt$ 162.2 eV $-SH$ (?) ~163.0 eV $-NH_2$ 400.8 eV $-NH_3{}^+$ 402.3 eV	UHV	Molecule is anchored to the surface by $S-Pt$ bond and it is mostly in zwitterionic phase.

Table 3.6. Literature review **(cont.)**

43	Ag(111)	L-cysteine	$-S-Ag$ 161.8-162.0 eV $-SH$ 164.4 eV $-NH_2$ 399.2 eV $-NH_3{}^+$ 402.0 eV	UHV	At RT L-cysteine chemisorbs via sulfur and forms a densely packed layer. In this layer molecules exists mainly as zwitterion. Annealing to 333 K leads to desorption of multilayer and one particular phase. Annealing to 390 K leads to another phase in which all functional groups interact with the surface.
44	Pt(111) FeO(111)/Pt(111) Fe_3O_4(111)/Pt(111)	L-cysteine	$-S-Pt$ 162 eV $-SH$ 164 eV $-NH_2$ 400.0 eV $-NH_3{}^+$ 401.5 eV	UHV	
45, 46	Ge(100)	L-cysteine L-methionine	$-SCH_3$ 161.8 eV $-S-Ge\,(1)$ 161.9 eV $-S-Ge\,(2)$ 162.9 eV $-SH$ 163.9 eV $-NH_2-Ge$ 398.7 eV $-NH_3{}^+$ 400.1 eV	UHV	L-cysteine adsorbs to the Ge surface through all three functional groups and thiolates are observed on the surface. L-methionine adsorbs to the surface intact, that is, $S-CH_3$ bond is not broken.
47	Cu(111)	L-methionine	$-NH_2$ 399.5 eV $-NH_3{}^+$ 401.3 eV	UHV	
48	Au(111)	L-methionine D-methionine	$-SCH_3$ 164.0 eV $-NH_3{}^+$ 401.6 eV	UHV	Molecules adsorbed on to the surface as zwitterions and up to a monolayer no significant differences have been observed for the XPS spectra.
49	Si(111)	L-methionine	$-NH_2-Si$ 398.7 eV $-NH_2\ldots H$ 401.1 eV $-NH_3{}^+$ 401.8 eV	UHV	
50	Pyrite(100)	L-cystine	$-NH_2$ 399.9 eV $-NH_3{}^+$ 401.8 eV	UHV	

The XPS literature for L-cysteine adsorption on Au surfaces shows that the first layer of the molecules chemisorbs to the metal surface through their dissociated thiol group ($-SH$) as thiolates ($-S-Metal$) [31–38]. The binding energy for the S $2p_{3/2}$ level for this species is around 161.5–162.3 eV. Starting from the second layer onwards and in some cases even before the first layer is completed, a physisorbed layer with intact thiol groups is formed and S $2p_{3/2}$ level binding energies for these species is around 163.8–164.4 eV[31–38]. Adsorption behavior for L-cysteine on Ag and Pt surfaces is similar to adsorption to Au surfaces, that is, the molecule binds to the surface through dissociated thiol group.[42–44]

Interaction between L-cysteine molecules and the Cu surfaces is slightly different from the Au surfaces. L-cysteine also binds to Cu as thiolates but in addition to sulfur-metal bond both amino and carboxylic functional groups interact with the surface.[31,33,39–41] In two of the studies it was showed that L-cysteine dissociated and atomic sulfur was observed on the surface.[40,41]

The number of XPS studies is for L-methionine is quite small compared with the studies for L-cysteine. The literature shows that L-methionine often adsorbs to different surfaces through more than one functional group[40,41,45,46] and $S-CH_3$ bond scission efficiencies and $S-Metal$ bond formation upon adsorption depend on the material and surface orientation. On Au(111) surface, L-methionine (and its enantiomer D-methionine) molecules stay intact and form rows of dimers. For this particular surface, it seems that intermolecular interactions are stronger than the molecule-surface interactions.[48] But on some surfaces, for example Cu(110)[40], $S-CH_3$ bond breaks easily and $S-Cu$ bond is formed.

Best to our knowledge there are only two XPS studies concerning the adsorption of L-cystine: one on Cu(110)[40] surface and the other is on Pyrite(100) surface.[50] On Cu(110) surface disulfide bond ($S-S$) breaks and the molecule adsorbs onto the surface as thiolates.

The results for amino groups for all three sulfur containing amino acids are rather different. Some researchers observed only protonated amino groups ($-NH_3^+$) for molecules on the surface[31] whereas some other researchers observed both protonated and neutral amino groups ($-NH_2$) for sub-monolayer and monolayer coverages.[33] On Cu(110) surface zwitterions are formed by only L-cysteine molecules while for both L-methionine and L-cystine neutral molecules are observed.[40] Although, the amount of both

species differ depending on coverage and the substrate, one common point is that both species are often observed on different surfaces for different coverages. The N 1s binding energies for the neutral amino groups are in 399.2–400.8 eV range and for protonated amino groups reported N 1s binding energies are in the range of 401.2–402.3 eV.

There are four XPS studies in literature that are concerned with similar question as we did. In the following paragraphs we discuss their results.

Firstly, Abdou et al[44] studied the adsorption and thermal stability of L-cysteine on of Pt (111), FeO(111)/Pt(111) and Fe_2O_3(111)/Pt(111) surfaces. In line with literature, the authors observed two components in the S 2p region. They assigned 164.0 eV component to intact thiol groups and 162.0 eV with dissociated thiols attached to the surface. For the N 1s measurement the authors also observed two components; the component with 400.0 eV binding energy is assigned to $-NH_2$ groups and the component with 401.5 eV binging energy to $-NH_3{}^+$ groups.

After multilayer measurement of L-cysteine, they studied monolayer L-cysteine on Pt{111} surface and investigated the change in spectra with temperature. The initial deposition of L-cysteine was made at 160 K. At this temperature, L-cysteine stayed intact on Pt{111} surface. Partial deprotonation happens on amino group. The interaction between L-cysteine and the surface is happening without breaking bonds on amino acid. After that, temperature was increased and higher temperature measurements were made to study thermal stability. L-cysteine shows decomposition on room temperatures. Dehydrogenation, decarboxylation, decarbonylation and deamination were observed. The interaction between Pt{111} surface and L-cysteine mainly happen by carboxylate and amino groups on room temperature. The second substrate FeO(111)/Pt(111) has been reproduced by monolayer coverage of Pt{111} surface. When monolayer L-cysteine at this surface investigated at low temperature it has been observed spectra stay similar to multilayer L-cysteine and it has been suggested that L-cysteine stays intact and absorption is happening in molecular form. When temperature was increased up to the room temperature, C 1s signal on 289 eV lost and a new S 2p 162 eV signal has been formed. This change was interpreted as the FeO and thiolate group interaction. And finally, for Fe_3O_4 (111)/Pt(111) surface four cycle of coverage has been applied. FeO layer has reached to 8 nm thickness. Pt(111) surface effect on L-cysteine is negligible for this system. Even on low temperature 162 eV S 2p peak appeared. Thiol binding is enhanced compared to FeO (111)/Pt(111). For this surface, main adsorption group is carboxylate and thiol group is binding to surface from defects.

In two different studies, Park et al [45] and Yang et al[46] have studied L-cysteine and L-methionine on Ge(100) surface. In both studies, the spectral changes were compared for different coverage values. At L-cysteine case at low coverage, bonds C and H with S break and atomic sulfur forms. Hydrogen atom makes bound with C and they form CH_2. Amine and carboxyl groups also play role in the adsorption. For the L-methionine case no bond breaking was observed on the thiol group and CH_3S adsorbs as a whole to the Ge (100). While it is observed that O-H dissociation -N dative bond and -S dative bond are formed.

Finally, Kim et al [51] have investigated the sulfur containing amino acids L-cysteine, L-methionine and L-cystine on Cu(110) surface. For the L-cysteine Cu(110) surface system it was observed that L-cysteine rearranges its binding sites with coverage amount. Rearrangement was observed on the L-cysteine on Cu (110) system, depending on coverage. Similar to Cu(531) surface at low coverage all functional groups of L-cysteine molecule are attached to the surface. When coverage increases one of the thiolate or carboxylate gains a H atom and loses its bond to the surface. At high populations only thiol group stays adsorbed to the surface. On the other hand, L-methionine and L-cystine form a stronger sulfur bond and amino or carboxylic group show no zwitterionic form.

3.3 Discussion

For every molecule-substrate system we studied we observed two components in the N 1s region. The low binding energy component was marked as N1 and the high binding energy component was marked as N2. The binding energy values for all N1 components (399.5-400.5 eV) were within the range that is reported in literature (399.2-400.8 eV) for amino groups ($-NH_2$) of amino acids. Therefore, we assign N1 component to amino groups. However, the binding energy values for N2 components are within the literature values (401.2-402.3 eV) for protonated amino groups ($-NH_3{}^+$) only for L-methionine/Cr (401.8-402.1 eV) system. The binding energy values for L-cystine/Fe (402.2-402.6 eV) and L-cysteine/Cr (402.3-402.9 eV) start from values close to literature values but shift to higher energies with increasing coverage. For L-cystine/Cr system N2 binding energy (402.7 eV) is slightly higher than the literature values. On the contrary, for L-methionine/Fe system N2 binding energy values (400.9-401.1 eV) are lower than the literature values.

The relative quantities for N1 and N2 species are different for different systems. For L-cysteine/Cr and L-methionine/Cr systems the relative amount of N2 component is higher and it increases with coverage. The increase in relative amount of N2 component with coverage is also observed for L-cysteine/Fe system but the relative amount of N1 component stays higher than N2. L-methionine/Fe system is completely different from all other cases in that there is no N1 component for the lowest coverage and as the coverage increases N1 components shows up and goes higher in relative intensity. For L-cystine/Cr system relative amount of N2 component is higher than N1 component but we cannot comment on the effect of coverage on relative intensities because we only performed one measurement for single coverage value.

In S 2p region we observed a single component, marked as S1, for all systems except L-cysteine/Fe. For the highest coverage we studied, a high binding energy component, marked as S2, appeared in S 2p spectrum of L-cysteine/Fe system. $2p_{3/2}$ binding energy values for S1 component of L-cysteine/Fe system (163.9 eV) fits with literature values reported for intact thiol ($-SH$) species. However, the binding energy for S2 component (166.0 eV) is higher than any binding energy value reported for amino acid/metal studies. For L-cysteine/Cr system the binding energy for S1 component (164.4-165.1 eV) starts from a value similar to thiol species but shifts to higher binding energies with increasing coverage (same behavior is observed for N2 component). The S1 components for both L-methionine/Cr system (164.0 eV) and L-methionine/Fe system (163.0 eV) fits with literature values for ($-SCH_3$).

In literature (Table 3.6) binding energy of the S 2p peak for sulfur atoms bonded to metal surfaces are in 161.5-162.3 eV range and we do not observe any signal in that binding energy region. This could be explained in two ways. One explanation is that molecular layers are so thick that photoelectrons from the molecule-surface interface cannot reach to the analyzer. However, we can dismiss this explanation right away because for all preparations we observed a signal from the elements of the substrate (Cr 2p Fe 3p, not shown). The other more likely explanation is that adventitious carbon and oxide layers partly or completely cover the metallic substrate so that molecules can interact with small number of metal atoms or do not have access to metal atoms at all. Nevertheless, different amino acids show different behavior on different substrates.

For the L-cysteine/Cr system both N1 and N2 components in N 1s region and S1 component in S 2p region shift to higher binding energy with increasing coverage. This can be explained as a final state effect in photoemission. We can speculate that as the

thickness of the molecular layer increases, the layer transforms into a more insulating character so that the core hole created by photoemission is not perfectly screened. This causes photoelectrons to be attracted to the core hole and a decrease in kinetic energy, that is, an increase in binding energy. Therefore, in line with literature, we assign N1 peak to $-NH_2$, N2 peak to $-NH_3{}^+$ and S1 peak to $-SH$ groups.

For the L-cysteine/Fe system we only studied 0.01 M and 0.02 M concentrations. The most interesting observation for this system is the 166.0 eV binding energy component in S 2p region which has not been observed before in any amino acid-metal studies. However the binding energy is close to the value reported for $-SO_x$ species by Lindberg et al.[52]. It could be the case, above a certain threshold concentration there is an oxidation mechanism for the L-cysteine/Fe system together with the water solvent. The binding energy of the S1 component is in line with the literature values for $-SH$ species and accordingly we assign S1 component to intact thiol group of the molecules. The other interesting observation is for N2 component in N 1s region in that although binding energy for both N1 and S1 components does not change, N2 component shifts to higher binding energy with increasing coverage. This cannot be explained as a final state effect as in the case for L-cysteine/Cr system because such an effect would cause all peaks to shift to high binding energy. One reasonable explanation could be that another amino related species with high binding energy emerges for the last concentration. However as of now we do not have an explanation for this observation.

For L-methionine/Cr system binding energies of the two components in N 1s region fit perfectly with literature values for to $-NH_2$ and $-NH_3{}^+$ species. Therefore, we assign these components to amino and protonated amino species. The S1 component in S 2p region also fits with the value reported by Humblot et al.[48] for intact $-SCH_3$ species. For this system we did not observe any shift in binding energy of the any components.

We observed two interesting points for L-methionine/Fe system. First interesting observation is that in the N 1s region there is only one component, N2, with binding energies values in line with $-NH_3{}^+$ species. Starting from the second higest coverage N1 component emerged and increased in relative intensity compared to N2 species. The binding energy is in line with literature values for $-NH_2$. Best to our knowledge such a behavior is observed for the first time. The more common observation is the opposite one, that is, $-NH_3{}^+$ species increase with coverage compared to $-NH_2$. The second interesting point related to the binding energy for the S1 components for L-methionine/Cr

and L-methionine/Fe systems. For both systems the S1 component is assigned to $-SCH_3$ species in line with literature. However, there is approximately 1 eV difference in binding energy between two components. We speculate that for L-methionine/Cr system, where 163.0 eV binding energy S1 component is observed, sulfur atom of the intact $-SCH_3$ group forms some kind of coordination bonding with Cr atoms of the surface.

For L-cystine/Cr system we could only study one coverage, saturated solution, with one substrate, chromium. Similar to the other systems we observed two components in N 1s region and assigned N1 component to $-NH_2$ and N2 component to $-NH_3{}^+$ species. The only sulfur component S1 has a relatively higher binding energy 165 eV which we assign intact disulfide ($-S-S-$) bonds of the cystine molecule.

CHAPTER 4

CONCLUSIONS

We have studied adsorption of three sulfur-containing amino acids, L-cysteine, L-methionine and L-cystine from solution with three different concentrations on two different substrates, iron and chromium. The polycrystalline Fe and Cr substrates had certain amount of carbon and oxygen contamination due to exposure to ambient conditions. We did not try to clean the substrates because our aim was to study *ex situ* molecule adsorption.

For L-cysteine molecules on Cr and Fe substrates we observed intact thiol groups, amino groups and protonated amino groups on the surface. In S 2p region of the L-cysteine/Fe system for the highest concentration of solution we observed a high binding energy component which is assigned to $-SO_x$ species. This kind of oxidation process has not been reported before in any XPS study for amino acid-surface interactions. In the N 1s region of the same system a component on the higher binding energy side of protonated amino groups may be emerging but as of now we do not have an explanation for this species.

Similar to the case for L-cysteine adsorption, for L-methionine molecules on Cr and Fe substrates we observed intact thiol, amino and protonated amino groups on the surface. There is an approximately 1 eV difference in S 2p binding energies for $-SCH_3$ species for L-methionine molecules on different substrates. We speculate that the low binding energy component, that is for L-methionine/Fe system, corresponds to intact $-SCH_3$ groups interacting with metal atoms on the surface. Another interesting observation for L-methionine/Fe system is the increase in relative intensity of amino groups compared with protonated amino groups with increasing coverage. In literature only the opposite behavior is observed.

For L-cystine/Cr system, similar to previous systems, amino and protonated amino groups together with intact disulfide bonds are observed on the surface.

We did not observe any signal from sulfur metal bond. We explain this as a result of adventitious carbon and oxygen species on the surface. We suggest that the molecules

have little or no access to metal atoms on the surface because of carbon any oxygen contamination. However, different substrates caused some differences for sulfur containing amino acid adsorption.

REFERENCES

(1) *WHO Director-General's opening remarks at the media briefing on COVID-19 - 11 March 2020*. https://www.who.int/director-general/speeches/detail/who-director-general-s-opening-remarks-at-the-media-briefing-on-covid-19---11-march-2020 (accessed 2022-05-05).

(2) Racaniello, V. R.; Flint, J.; Skalka, A. M.; Rall, G. F.; Hatziioannou, T. *Principles of Virology*.

(3) Tortora, G. J.; Funke, B. R.; Case, C. L. *Microbiology: An Introduction*, Thirteenth edition, global edition.; Pearson: Harlow, 2021.

(4) Mahy, B. W. J. *The Dictionary of Virology*, 4th ed.; Elsevier, Academic Press: Amsterdam Heidelberg, 2009.

(5) Louten, J. Virus Structure and Classification. In *Essential Human Virology*; Elsevier, 2016; pp 19–29. https://doi.org/10.1016/B978-0-12-800947-5.00002-8.

(6) Barker, J.; Stevens, D.; Bloomfield, S. F. Spread and Prevention of Some Common Viral Infections in Community Facilities and Domestic Homes. *J. Appl. Microbiol.* **2001**, *91* (1), 7–21. https://doi.org/10.1046/j.1365-2672.2001.01364.x.

(7) *Modes of transmission of virus causing COVID-19: implications for IPC precaution recommendations*. https://www.who.int/news-room/commentaries/detail/modes-of-transmission-of-virus-causing-covid-19-implications-for-ipc-precaution-recommendations (accessed 2022-05-09).

(8) van Doremalen, N.; Bushmaker, T.; Morris, D. H.; Holbrook, M. G.; Gamble, A.; Williamson, B. N.; Tamin, A.; Harcourt, J. L.; Thornburg, N. J.; Gerber, S. I.; Lloyd-Smith, J. O.; de Wit, E.; Munster, V. J. Aerosol and Surface Stability of SARS-CoV-2 as Compared with SARS-CoV-1. *N. Engl. J. Med.* **2020**, *382* (16), 1564–1567. https://doi.org/10.1056/NEJMc2004973.

(9) Lewis, D. COVID-19 Rarely Spreads through Surfaces. So Why Are We Still Deep Cleaning? *Nature* **2021**, *590* (7844), 26–28. https://doi.org/10.1038/d41586-021-00251-4.

(10) Ijaz, M. K.; Nims, R. W.; McKinney, J. Indirect Transmission of Severe Acute Respiratory Syndrome Coronavirus Virus 2 (SARS-CoV-2): What Do We Know and What Do We Not Know? *Infect. Control Hosp. Epidemiol.* **2022**, *43* (5), 676–678. https://doi.org/10.1017/ice.2021.57.

(11) Fehr, A. R.; Perlman, S. Coronaviruses: An Overview of Their Replication and Pathogenesis. In *Coronaviruses*; Maier, H. J., Bickerton, E., Britton, P., Eds.; Methods in Molecular Biology; Springer New York: New York, NY, 2015; Vol. 1282, pp 1–23. https://doi.org/10.1007/978-1-4939-2438-7_1.

(12) Huang, Y.; Yang, C.; Xu, X.; Xu, W.; Liu, S. Structural and Functional Properties of SARS-CoV-2 Spike Protein: Potential Antivirus Drug Development for COVID-19. *Acta Pharmacol. Sin.* **2020**, *41* (9), 1141–1149. https://doi.org/10.1038/s41401-020-0485-4.

(13) Mariano, G.; Farthing, R. J.; Lale-Farjat, S. L. M.; Bergeron, J. R. C. Structural Characterization of SARS-CoV-2: Where We Are, and Where We Need to Be. *Front. Mol. Biosci.* **2020**, *7*, 605236. https://doi.org/10.3389/fmolb.2020.605236.

(14) Malaspina, D. C.; Faraudo, J. Computer Simulations of the Interaction between SARS-CoV-2 Spike Glycoprotein and Different Surfaces. 11.

(15) Choppin, P. W.; Scheid, A. The Role of Viral Glycoproteins in Adsorption, Penetration, and Pathogenicity of Viruses. *Rev. Infect. Dis.* **1980**, *2* (1), 40–61.

(16) Artemenko, A.; Shchukarev, A.; Štenclová, P.; Wågberg, T.; Segervald, J.; Jia, X.; Kromka, A. Reference XPS Spectra of Amino Acids. *IOP Conf. Ser. Mater. Sci. Eng.* **2021**, *1050* (1), 012001. https://doi.org/10.1088/1757-899X/1050/1/012001.

(17) Ambrogelly, A.; Palioura, S.; Söll, D. Natural Expansion of the Genetic Code. *Nat. Chem. Biol.* **2007**, *3* (1), 29–35. https://doi.org/10.1038/nchembio847.

(18) Townsend, D. M.; Tew, K. D.; Tapiero, H. Sulfur Containing Amino Acids and Human Disease. *Biomed. Pharmacother.* **2004**, *58* (1), 47–55. https://doi.org/10.1016/j.biopha.2003.11.005.

(19) Brosnan, J. T.; Brosnan, M. E. The Sulfur-Containing Amino Acids: An Overview. *J. Nutr.* **2006**, *136* (6), 1636S-1640S. https://doi.org/10.1093/jn/136.6.1636S.

(20) Stevie, F. A.; Donley, C. L. Introduction to X-Ray Photoelectron Spectroscopy. *J. Vac. Sci. Technol. A* **2020**, *38* (6), 063204. https://doi.org/10.1116/6.0000412.

(21) Steinhardt, R.; Serfass, E. X-Ray Photoelectron Spectrometer for Chemical Analysis. *Anal. Chem.* **1951**, *23* (11), 1585–1590. https://doi.org/10.1021/ac60059a019.

(22) Ashcroft, N. W.; Mermin, N. D. *Solid State Physics*; Holt, Rinehart and Winston: New York, 1976.

(23) Andrade, J. D. X-Ray Photoelectron Spectroscopy (XPS). 91.

(24) Powell, C. J. Practical Guide for Inelastic Mean Free Paths, Effective Attenuation Lengths, Mean Escape Depths, and Information Depths in x-Ray Photoelectron

Spectroscopy. *J. Vac. Sci. Technol. A* **2020**, *38* (2), 023209. https://doi.org/10.1116/1.5141079.

(25) Tanuma, S.; Powell, C. J.; Penn, D. R. Proposed Formula for Electron Inelastic Mean Free Paths Based on Calculations for 31 Materials. *Surf. Sci. Lett.* **1987**, *192* (1), L849–L857. https://doi.org/10.1016/0167-2584(87)90829-2.

(26) Crist, B. V. *XPS PHYSICS*. https://en.wikipedia.org/wiki/File:XPS_PHYSICS.png (accessed 2022-06-27).

(27) *Handbook of X-Ray Photoelectron Spectroscopy: A Reference Book of Standard Spectra for Identification and Interpretation of XPS Data*, Update.; Moulder, J. F., Chastain, J., Eds.; Perkin-Elmer Corporation: Eden Prairie, Minn, 1992.

(28) Zhang, X.; da Silva, C. C.; Zhang, S.; Prabhakar, M.; Lu, W.; Vogel, A.; Rohwerder, M. Investigation of Selective Oxidation during Cooling of Hot-Rolled Iron-Manganese-Silicon Alloys. *Corros. Sci.* **2021**, *186*, 109466. https://doi.org/10.1016/j.corsci.2021.109466.

(29) Major, G. H.; Fairley, N.; Sherwood, P. M. A.; Linford, M. R.; Terry, J.; Fernandez, V.; Artyushkova, K. Practical Guide for Curve Fitting in X-Ray Photoelectron Spectroscopy. *J. Vac. Sci. Technol. A* **2020**, *38* (6), 061203. https://doi.org/10.1116/6.0000377.

(30) *Practical Surface Analysis: By Auger and x-Ray Photoelectron Spectroscopy*; Briggs, D., Seah, M. P., Eds.; Wiley: Chichester ; New York, 1983.

(31) Uvdal, K.; Bodö, P.; Liedberg, B. L-Cysteine Adsorbed on Gold and Copper: An X-Ray Photoelectron Spectroscopy Study. *J. Colloid Interface Sci.* **1992**, *149* (1), 162–173. https://doi.org/10.1016/0021-9797(92)90401-7.

(32) Filimon, A.-D.; Jacob, P.; Hergenröder, R.; Jürgensen, A. Study on the Reversible Changes of the Surface Properties of an L-Cysteine Self-Assembled Monolayer on Gold As a Function of PH. *Langmuir* **2012**, *28* (23), 8692–8699. https://doi.org/10.1021/la3013574.

(33) Jürgensen, A.; Raschke, H.; Esser, N.; Hergenröder, R. An in Situ XPS Study of L-Cysteine Co-Adsorbed with Water on Polycrystalline Copper and Gold. *Appl. Surf. Sci.* **2018**, *435*, 870–879. https://doi.org/10.1016/j.apsusc.2017.11.150.

(34) Dodero, G.; De Michieli, L.; Cavalleri, O.; Rolandi, R.; Oliveri, L.; Daccà, A.; Parodi, R. L-Cysteine Chemisorption on Gold: An XPS and STM Study. *Colloids Surf. Physicochem. Eng. Asp.* **2000**, *175* (1–2), 121–128. https://doi.org/10.1016/S0927-7757(00)00521-5.

(35) Cavalleri, O.; Oliveri, L.; Daccà, A.; Parodi, R.; Rolandi, R. XPS Measurements on L-Cysteine and 1-Octadecanethiol Self-Assembled Films: A Comparative Study. *Appl. Surf. Sci.* **2001**, *175–176*, 357–362. https://doi.org/10.1016/S0169-4332(01)00067-8.

(36) Cavalleri, O.; Gonella, G.; Terreni, S.; Vignolo, M.; Pelori, P.; Floreano, L.; Morgante, A.; Canepa, M.; Rolandi, R. High Resolution XPS of the S 2p Core Level Region of the L-Cysteine/Gold Interface. *J. Phys. Condens. Matter* **2004**, *16* (26), S2477–S2482. https://doi.org/10.1088/0953-8984/16/26/021.

(37) Gonella, G.; Terreni, S.; Cvetko, D.; Cossaro, A.; Mattera, L.; Cavalleri, O.; Rolandi, R.; Morgante, A.; Floreano, L.; Canepa, M. Ultrahigh Vacuum Deposition of L-Cysteine on Au(110) Studied by High-Resolution X-Ray Photoemission: From Early Stages of Adsorption to Molecular Organization. *J. Phys. Chem. B* **2005**, *109* (38), 18003–18009. https://doi.org/10.1021/jp051549t.

(38) Caprile, L.; Cossaro, A.; Falletta, E.; Della Pina, C.; Cavalleri, O.; Rolandi, R.; Terreni, S.; Ferrando, R.; Rossi, M.; Floreano, L.; Canepa, M. Interaction of L-Cysteine with Naked Gold Nanoparticles Supported on HOPG: A High Resolution XPS Investigation. *Nanoscale* **2012**, *4* (24), 7727. https://doi.org/10.1039/c2nr32741d.

(39) Kim, J. W.; Hwang, H.-N.; Hwang, C.-C. Adsorption of Cysteine on Cu(110) Studied by Core-Level Photoelectron Spectroscopy. *J. Phys. Chem. C* **2007**, *111* (35), 13192–13196. https://doi.org/10.1021/jp072496d.

(40) Kim, J. W.; Lee, Y. M.; Lee, S. M.; Son, M. J.; Kang, H.; Park, Y. Surface Reaction of Sulfur-Containing Amino Acids on Cu(110). *Langmuir* **2010**, *26* (8), 5632–5636. https://doi.org/10.1021/la904496j.

(41) Thomsen, L.; Wharmby, M. T.; Riley, D. P.; Held, G.; Gladys, M. J. The Adsorption and Stability of Sulfur Containing Amino Acids on Cu{531}. *Surf. Sci.* **2009**, *603* (9), 1253–1261. https://doi.org/10.1016/j.susc.2009.03.014.

(42) Stampfl, A. P. J.; Chen, C.-H.; Wang, S.-C.; Huang, M.-L.; Klauser, R. A Scanning Photoemission Microprobe Study of the Adsorption of Cysteine on Pt{111}. *J. Electron Spectrosc. Relat. Phenom.* **2005**, *144–147*, 417–420. https://doi.org/10.1016/j.elspec.2005.01.051.

(43) Fischer, S.; Papageorgiou, A. C.; Marschall, M.; Reichert, J.; Diller, K.; Klappenberger, F.; Allegretti, F.; Nefedov, A.; Wöll, C.; Barth, J. V. L-Cysteine on Ag(111): A Combined STM and X-Ray Spectroscopy Study of Anchorage and Deprotonation. *J. Phys. Chem. C* **2012**, *116* (38), 20356–20362. https://doi.org/10.1021/jp305270h.

(44) Abdou, J.-M.; Seidel, P.; Sterrer, M. Bonding and Thermal Stability of Cysteine on Single-Crystalline Iron Oxide Surfaces and Pt(111). *J. Chem. Phys.* **2020**, *152* (6), 064701. https://doi.org/10.1063/1.5143416.

(45) Park, S.; Yang, S.; Shin, N.; Lee, E.; Lee, H. Adsorption Configuration for Cysteine on Ge(100): Coverage-Dependent Surface Reorientation. *J. Phys. Chem. C* **2010**, *114* (34), 14528–14531. https://doi.org/10.1021/jp104029v.

(46) Yang, S.; Kim, Y.; Park, S.; Kim, K.; Lee, H. Coverage-Dependent Variation of Adsorption Configurations of Methionine on Ge(100). *Chem. – Asian J.* **2011**, *6*

(9), 2362–2367. https://doi.org/10.1002/asia.201100004.

(47) Schiffrin, A.; Reichert, J.; Pennec, Y.; Auwärter, W.; Weber-Bargioni, A.; Marschall, M.; Dell'Angela, M.; Cvetko, D.; Bavdek, G.; Cossaro, A.; Morgante, A.; Barth, J. V. Self-Assembly of l-Methionine on Cu(111): Steering Chiral Organization by Substrate Reactivity and Thermal Activation. *J. Phys. Chem. C* **2009**, *113* (28), 12101–12108. https://doi.org/10.1021/jp900593g.

(48) Humblot, V.; Tielens, F.; Luque, N. B.; Hampartsoumian, H.; Méthivier, C.; Pradier, C.-M. Characterization of Two-Dimensional Chiral Self-Assemblies l- and d-Methionine on Au(111). *Langmuir* **2014**, *30* (1), 203–212. https://doi.org/10.1021/la404262m.

(49) Rahsepar, F. R.; Leung, K. T. Surface Functionalization of Reconstructed Si(111) with Methionine. *J. Phys. Chem. C* **2019**, *123* (44), 26980–26988. https://doi.org/10.1021/acs.jpcc.9b07226.

(50) Sanchez-Arenillas, M.; Mateo-Marti, E. Pyrite Surface Environment Drives Molecular Adsorption: Cystine on Pyrite(100) Investigated by X-Ray Photoemission Spectroscopy and Low Energy Electron Diffraction. *Phys. Chem. Chem. Phys.* **2016**, *18* (39), 27219–27225. https://doi.org/10.1039/C6CP03760G.

(51) Kim, J. W.; Lee, Y. M.; Lee, S. M.; Son, M. J.; Kang, H.; Park, Y. Surface Reaction of Sulfur-Containing Amino Acids on Cu(110). *Langmuir* **2010**, *26* (8), 5632–5636. https://doi.org/10.1021/la904496j.

(52) Lindberg, B. J.; Hamrin, K.; Johansson, G.; Gelius, U.; Fahlman, A.; Nordling, C.; Siegbahn, K. Molecular Spectroscopy by Means of ESCA II. *Sulfur Compounds. Correlation of Electron Binding Energy with Structure*. *Phys. Scr.* **1970**, *1* (5–6), 286–298. https://doi.org/10.1088/0031-8949/1/5-6/020.